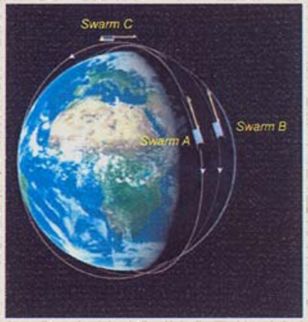

Low Latitude Ionospheric Studies using Satellite Magnetic Data

A. Bhattacharyya
Indian Institute of Geomagnetism

First *Swarm* International Science Workshop
Nantes, May 3 – 5, 2006

Outline:

- Equatorial plasma bubbles (EPBs)
- Observations of magnetic field fluctuations associated with EPBs
- Theoretical developments
- Evolution of EPBs during quiet periods
- EPBs associated with magnetic activity
- EPB related observations with ***Swarm***

Equatorial Plasma Bubbles

Development of an equatorial plasma bubble (EPB) on the bottomside of post-sunset equatorial ionospheric *F* region due to growth of the Rayleigh-Taylor (R-T) instability

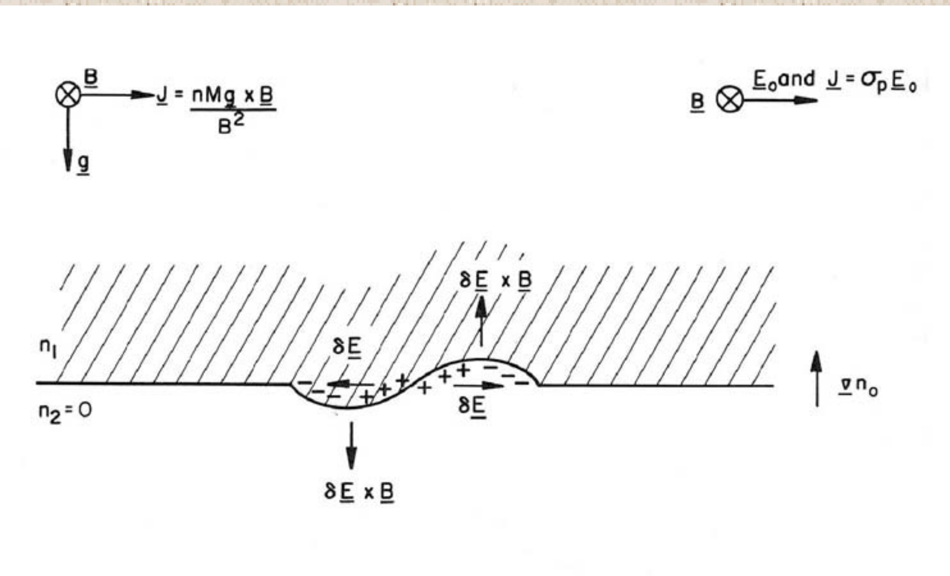

Nonlinear development of field aligned plasma bubble

Electrostatic R-T instability after approx. 1 hour (3D)

Densities normalized by $2.1 \times 10^{12}\ m^{-3}$ for the equator

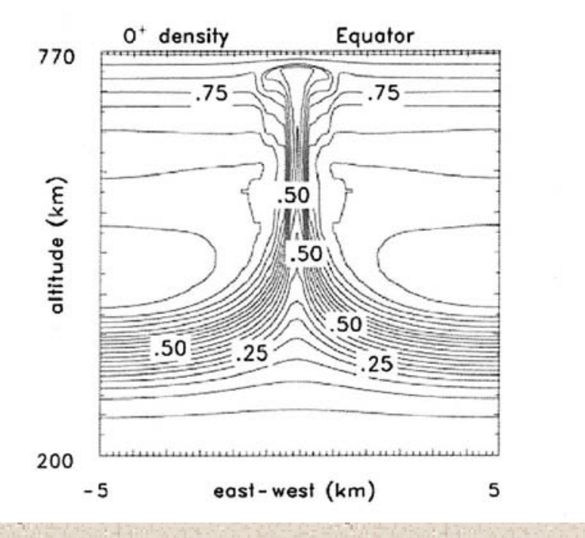

Densities normalized by $4.2 \times 10^{12}\ m^{-3}$ for the anomaly

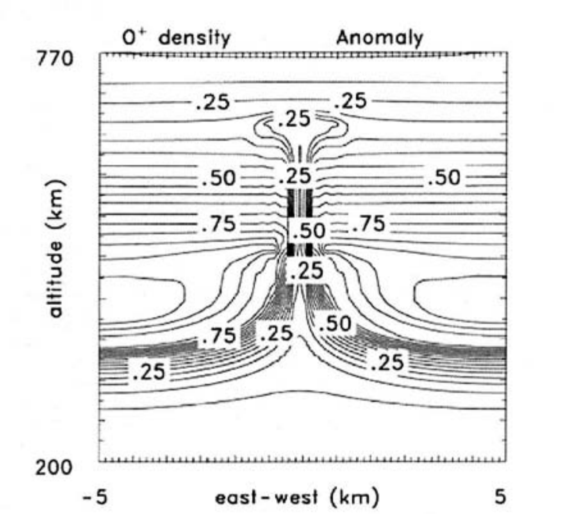

Keskinen et al., 2003

Coherent scatter radar observations of Equatorial Spread F

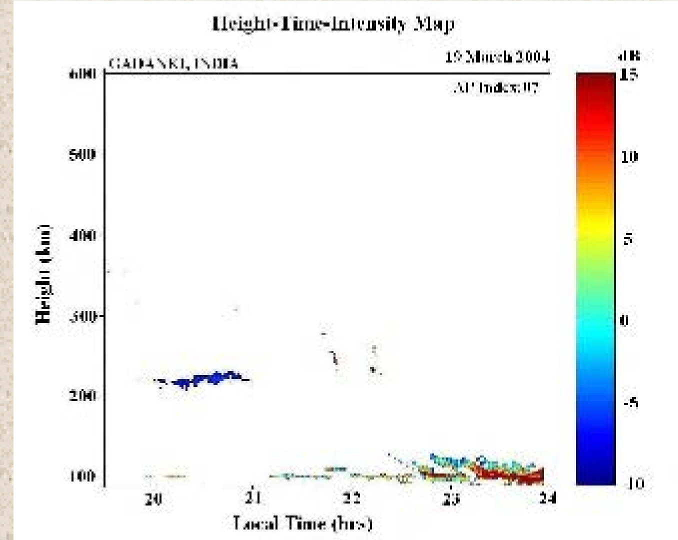

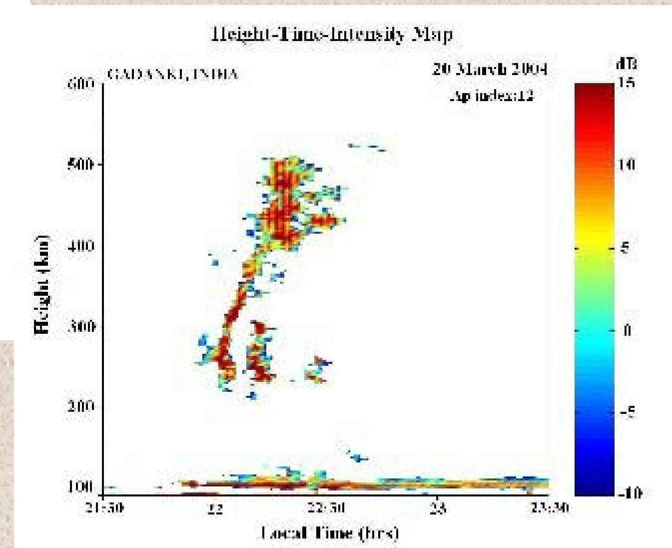

Day-to-day variability of equatorial spread F (ESF) phenomenon

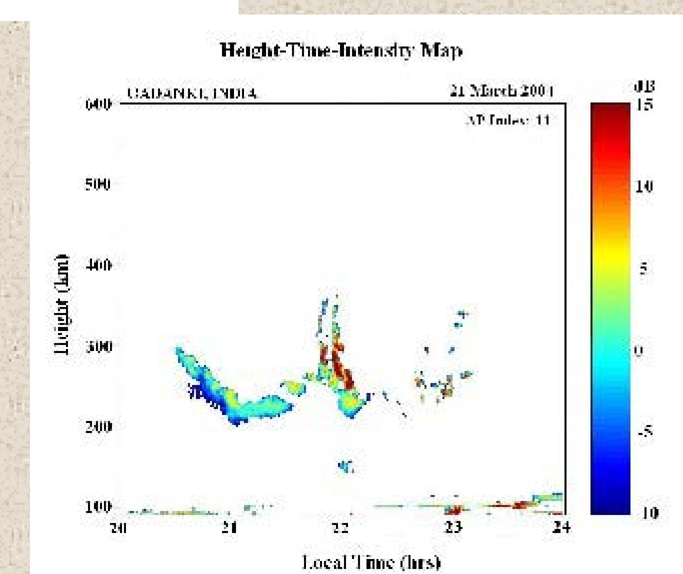

Scintillations on GPS signals due to EPBs

Intensity scintillations on GPS L1 signal

Simultaneous variations in total electron content (TEC) along the signal path

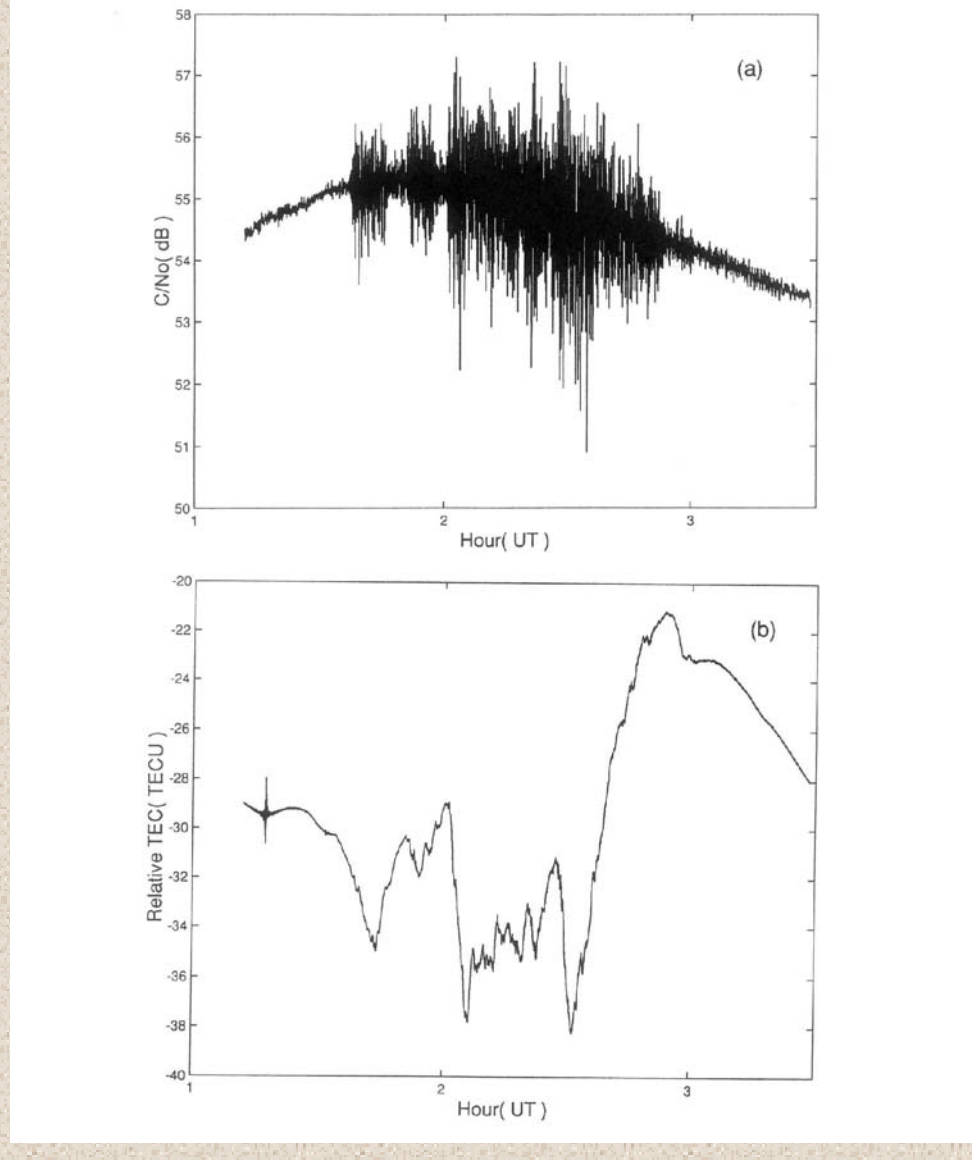

Bhattacharyya et al., 2000

When are scintillation-causing irregularities most likely to occur ?

To lowest order, seasonal dependence of equatorial/low latitude scintillation activity at a given longitude is controlled by the angle between the magnetic meridian and sunset terminator.

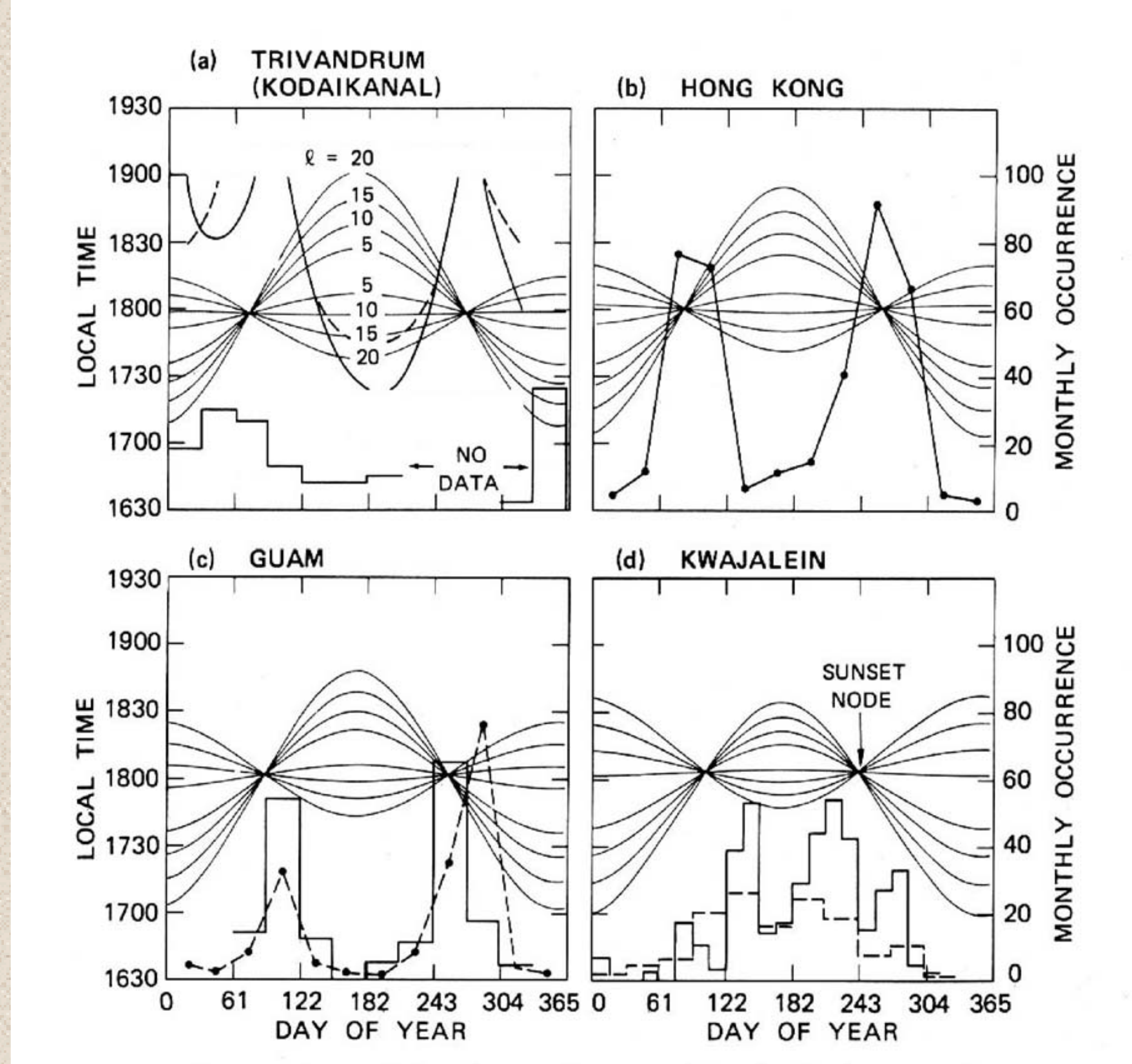

Tsunoda, 1985

Magnetic field fluctuation associated with a supersonic EPB observed by DE 2 on September 13, 1982, at an altitude of 402 km, geog. longitude of 305° (LT ~ 23), and magnetic latitude of –13.7°

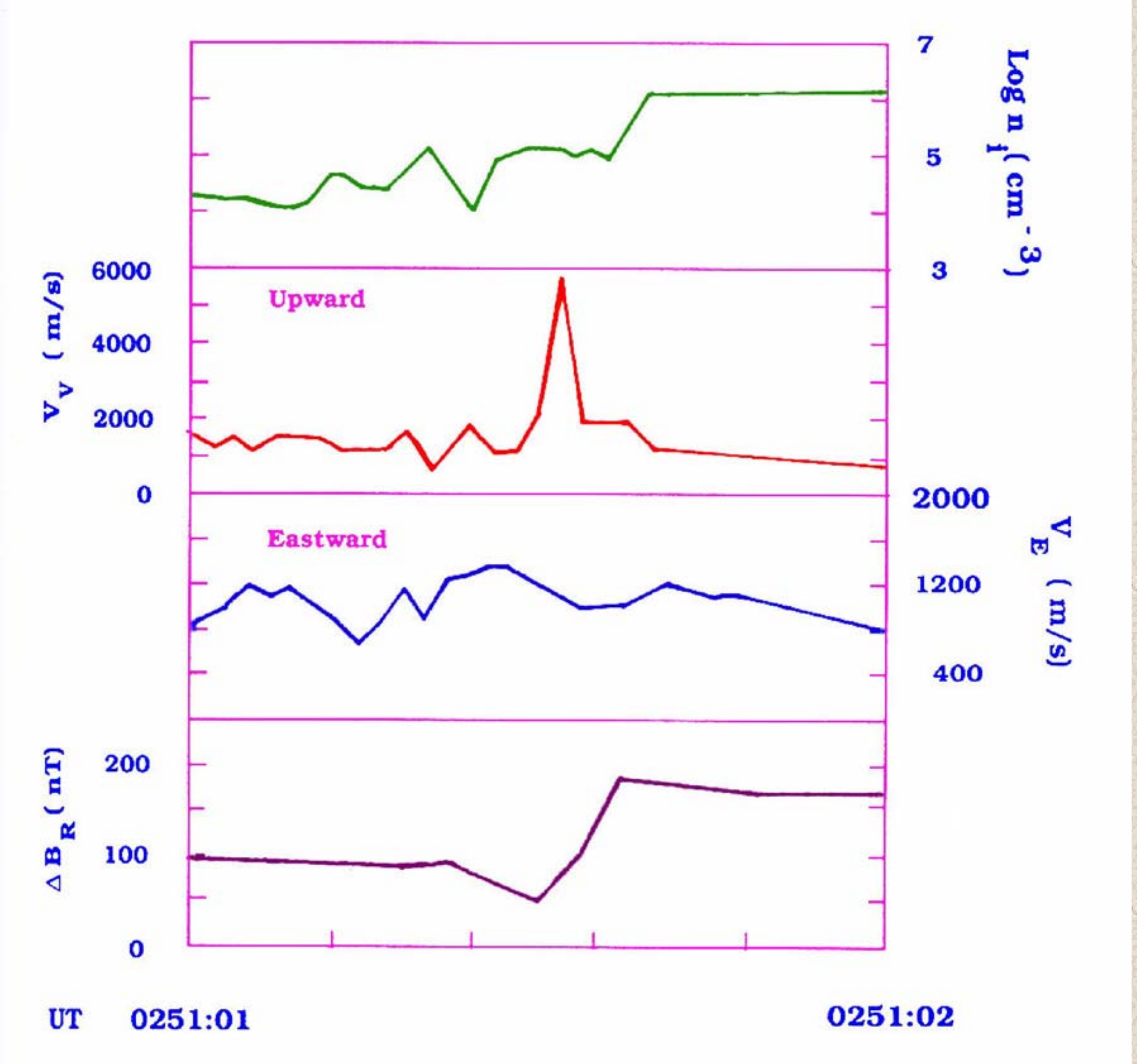

Aggson et al., 1992

Broadband electric and magnetic field intensities and plasma density measured by ELFWA instrument on CRRES during a perigee pass on October 7, 1991, at an altitude of 453 km and magnetic latitude of 6.2° N, at 02:45 LT . This was a magnetically disturbed day (Ap = 33).

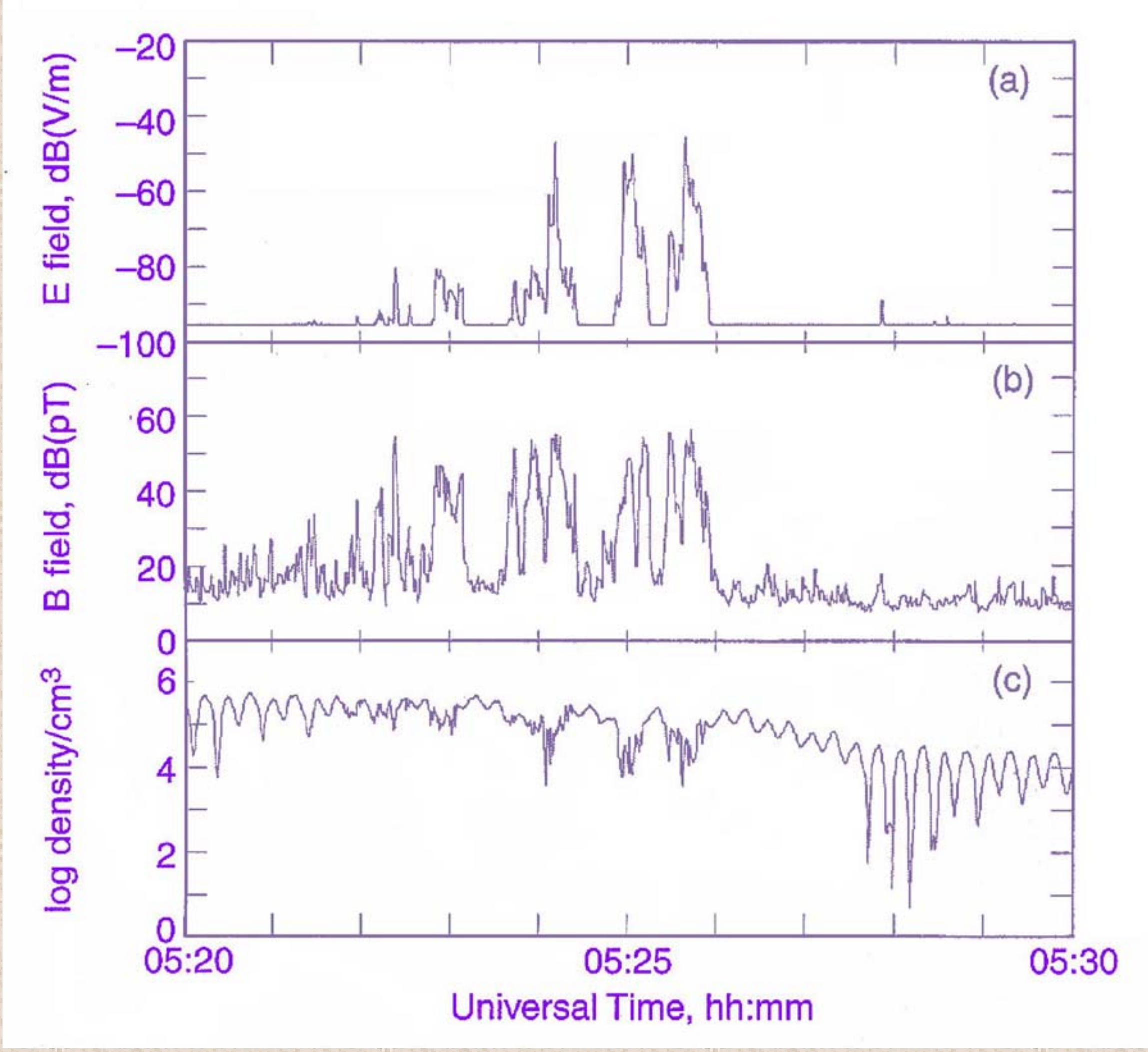

Koons et al., 1997

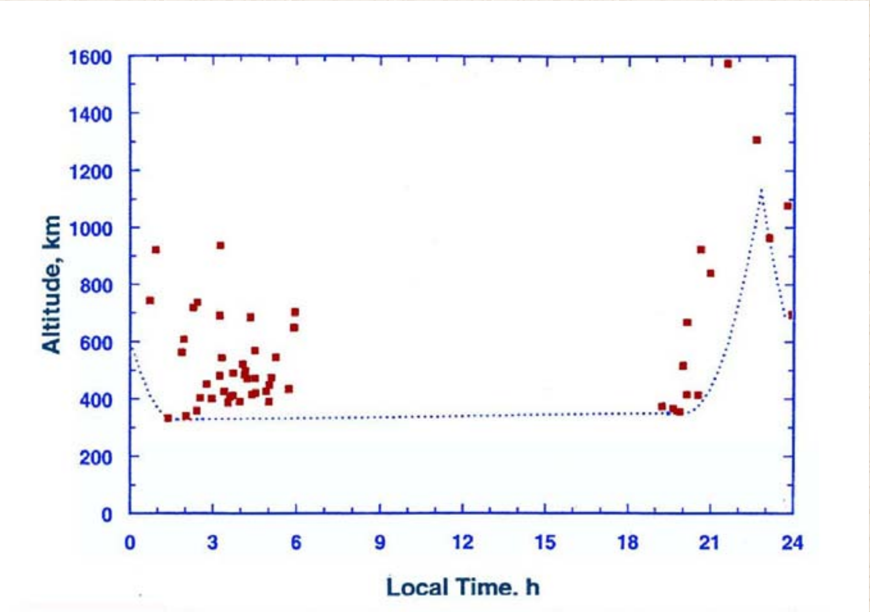

Locations in altitude and local time where EPB associated plasma waves were observed by CRRES

Refractive indices calculated from the observations:

$$n = c\,B/E$$

were consistent with the expected values of n_x, the refractive index for extraordinary mode, based on the observed electron densities in some of the cases.

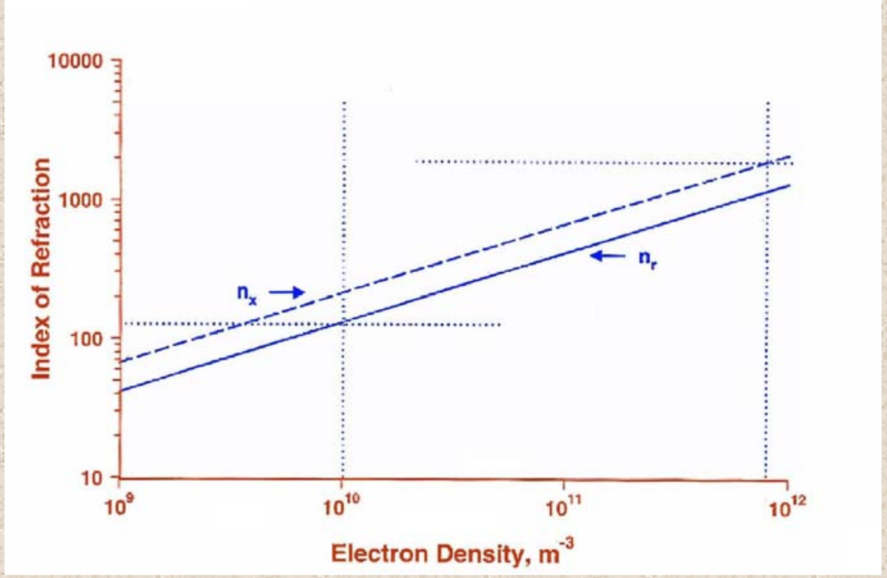

Koons et al., 1997

Stolle et al., 2006

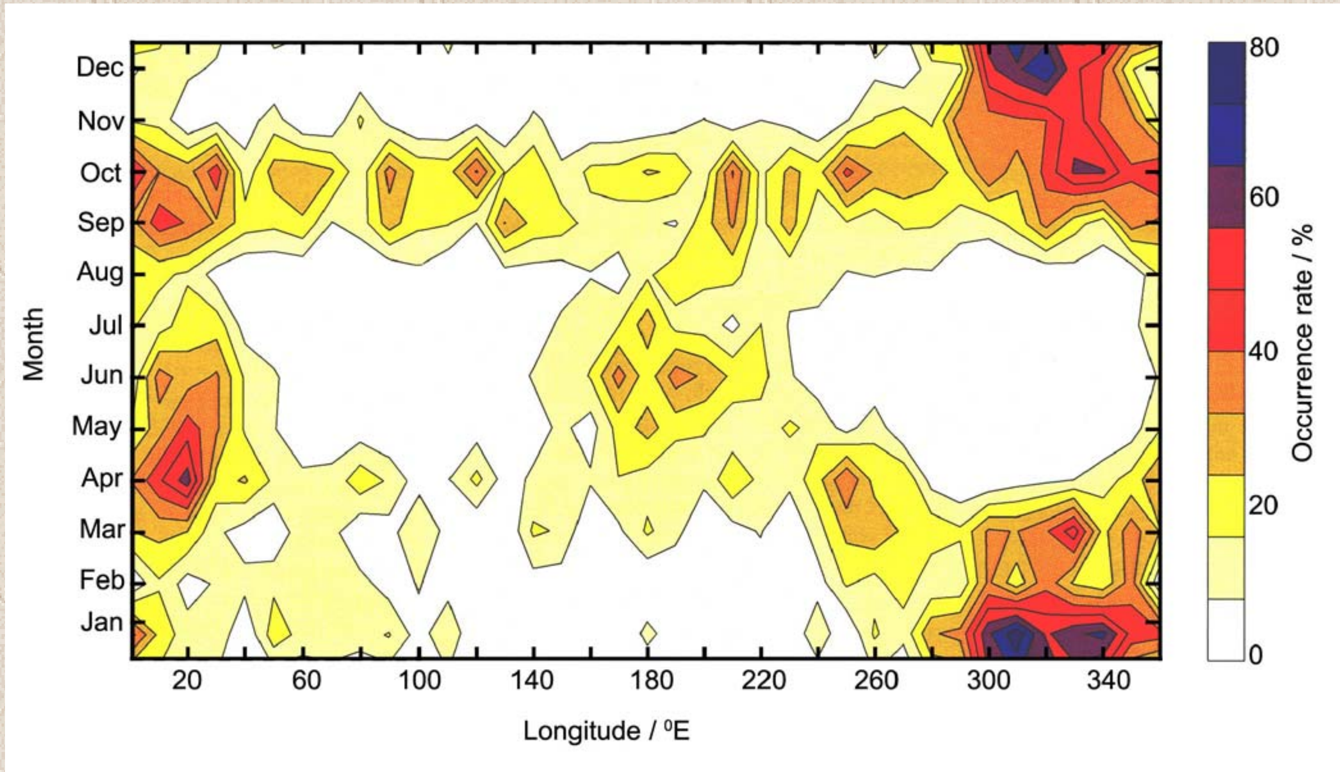

Occurrence rates of EPB associated magnetic signatures observed by CHAMP during 2001-2004 at an average altitude ~ 400 km

Burke et al., 2004

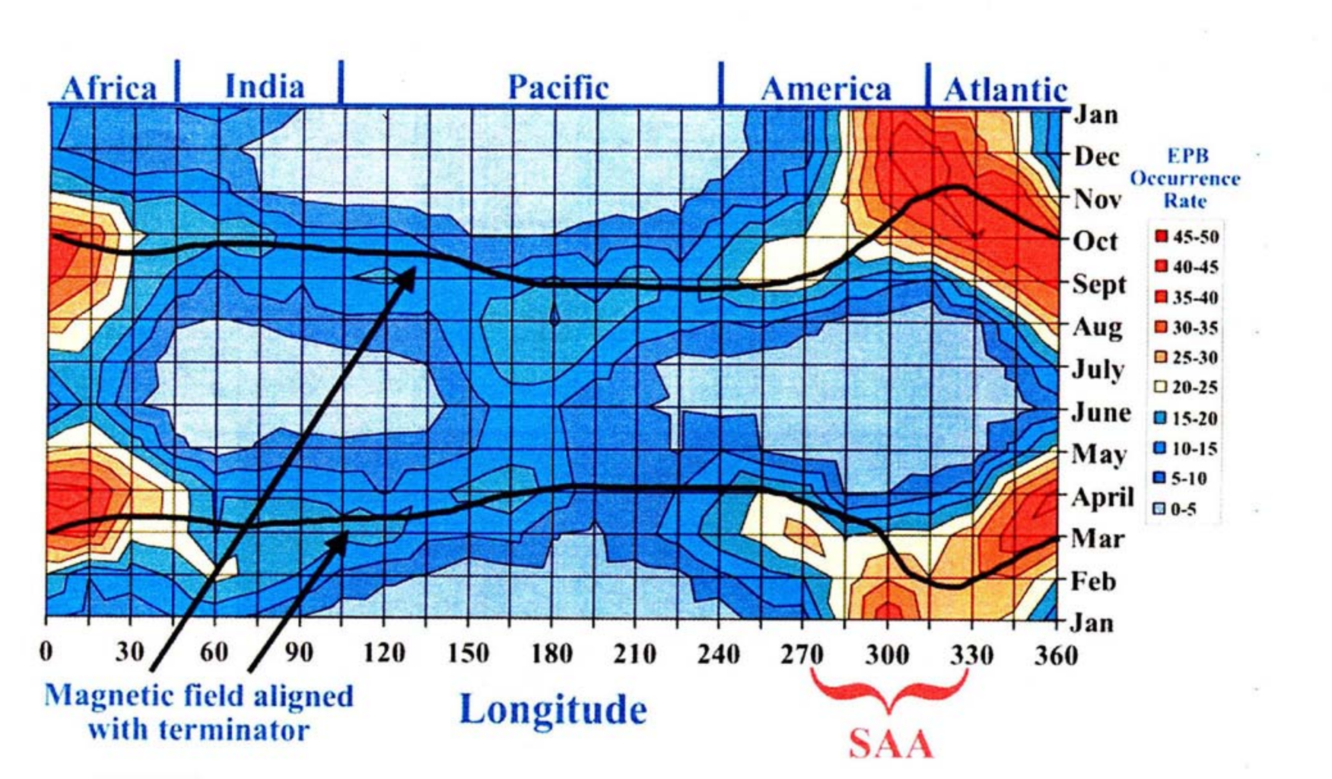

Occurrence rates of EPBs based on electron density measurements by DMSP salellites during 1989-2002 at an altitude ~ 840 km.

A possible mechanism for observed magnetic fluctuations

Shear Alfvén waves are generated as the equatorial plasma bubble starts to grow. These waves carry the field-aligned currents that couple the equatorial F region with conjugate E regions.

Transmission line analogy

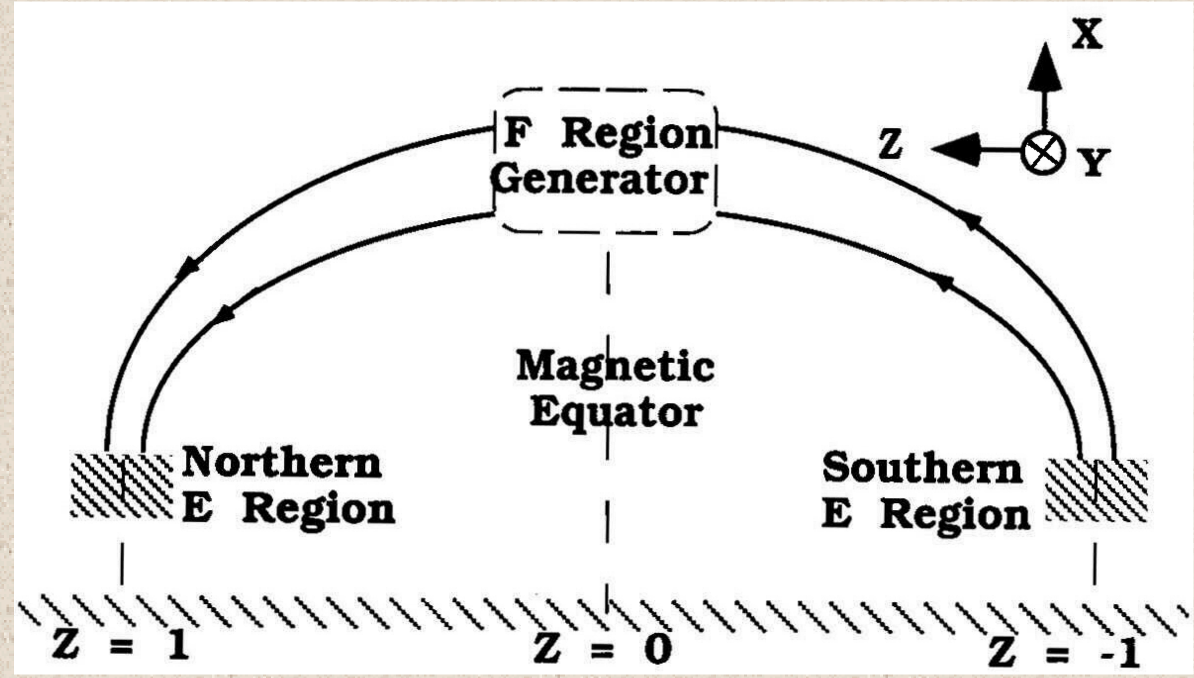

Condition for non-vanishing density perturbation:

$$\Sigma_{PN}^{E} = \Sigma_{PS}^{E} \approx 0$$

Bhattacharyya and Burke, 2000

Extension of the transmission line analogy to a 3-mode system to describe the non-linear evolution of EPBs through the growth of an electromagnetic Rayleigh-Taylor instability, yielded the following condition for development of topside structure is:

$$\nu_i + \underbrace{\frac{\mu_0 V_A^2 \Sigma_P^E}{l}} < \sqrt{\frac{g}{2L}}$$

Rate of discharge of the bubble through the conjugate E regions

Bhattacharyya, 2004

Electromagnetic R-T modes assuming:

- Ion inertia is negligible for field line apex altitude of 300 km.

- Finite parallel conductivity

E_ϕ is normalized to a value of 1 mV/m at the magnetic equator ($s = 0$)

$\hat{s} = s / l$

l = length of the field line

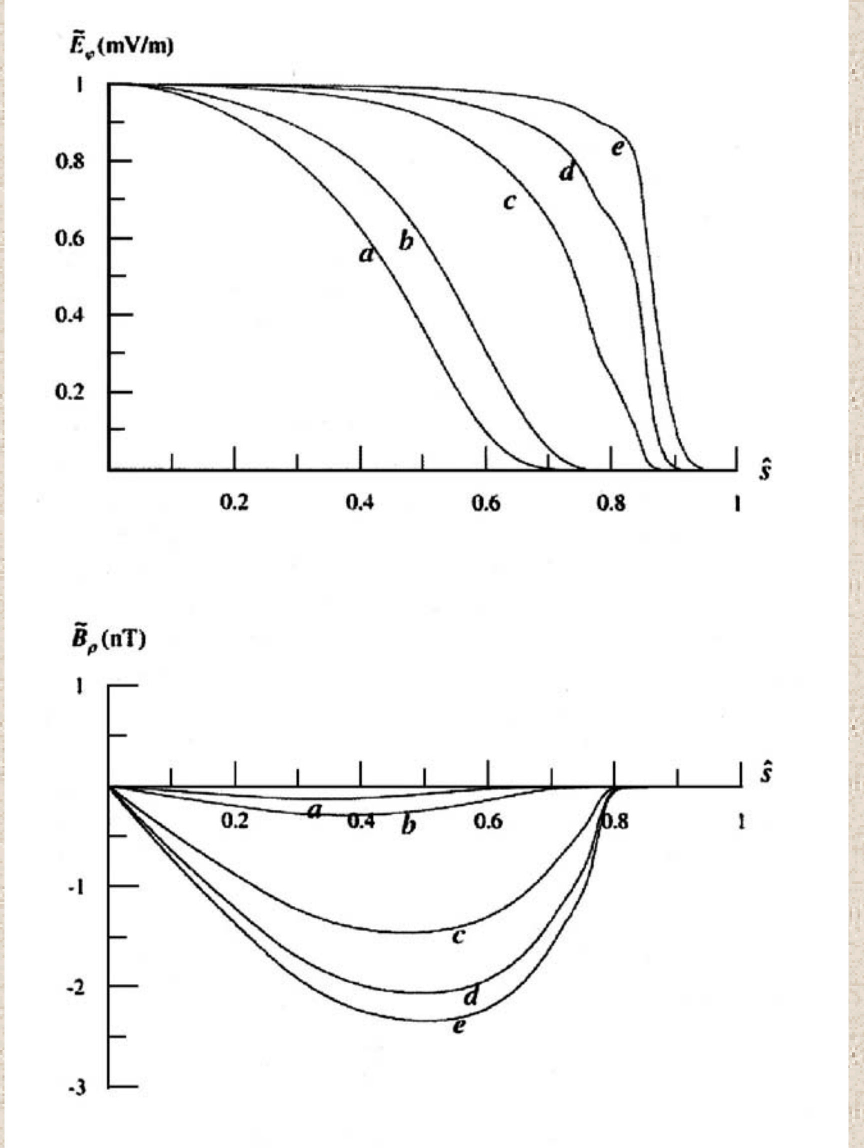

Basu, 2005

Evening prereversal enhancement of the equatorial F region vertical drift has emerged as an important factor in the generation and evolution of EPBs

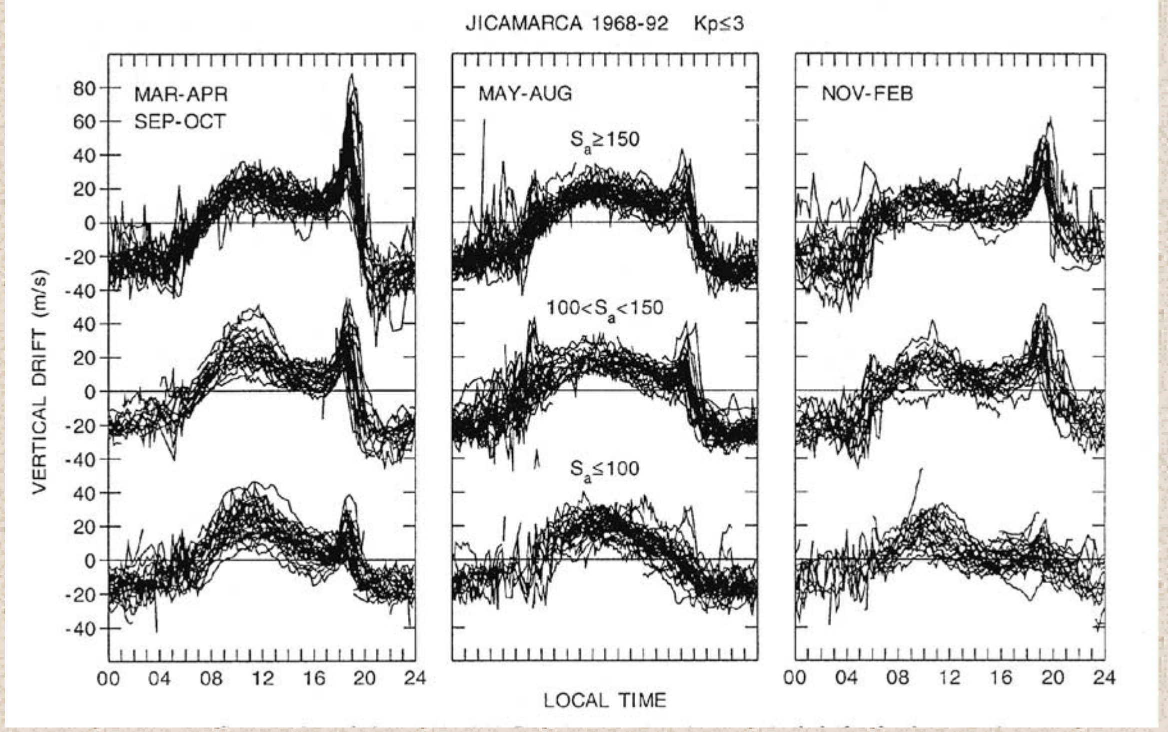

Scatterplot of the quiet time equatorial F region vertical drifts for low, medium, and high solar flux conditions obtained from incoherent scatter radar observations at Jicamarca during 1968-1992.

Scherliess and Fejer, 1999

Martinis et al., 2003

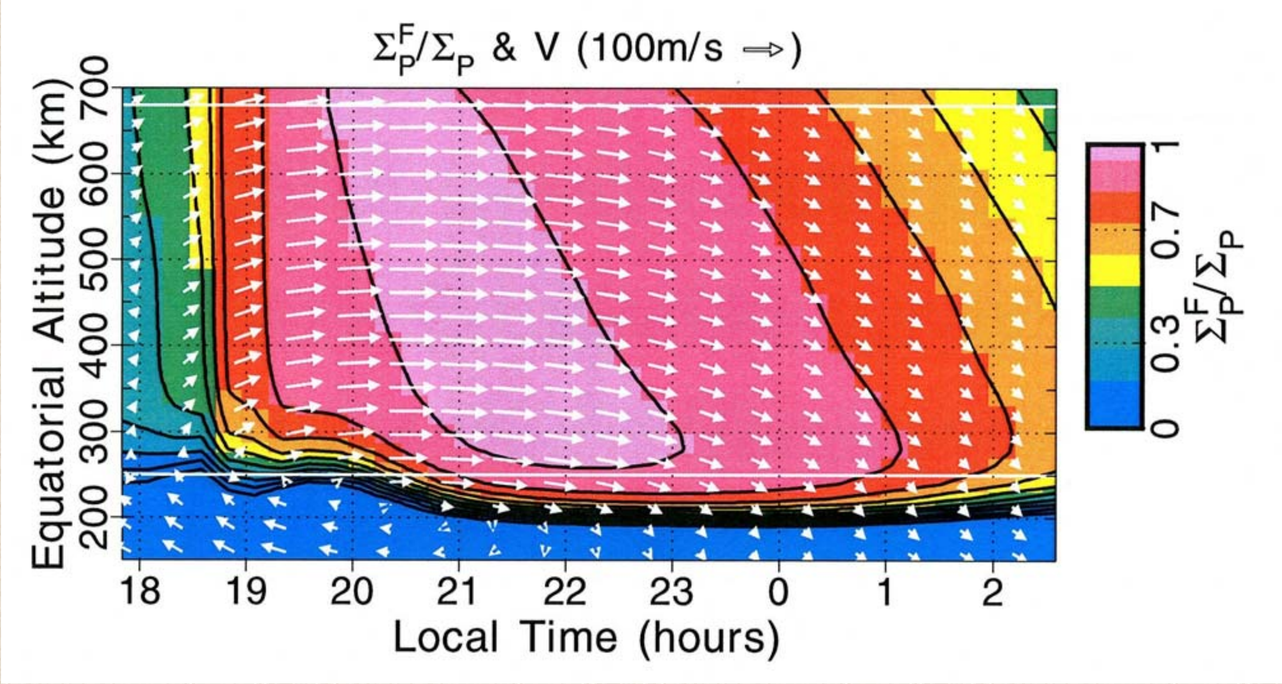

Model plasma drifts calculated in the magnetic equatorial plane show a vortex structure with the source residing on the bottomside of the F region. It has been suggested that the prereversal enhancement in the equatorial F region vertical drift is determined by this vortex structure (Eccles, 1999).

Is there a relationship with with low latitude ionospheric F region currents estimated from satellite data?

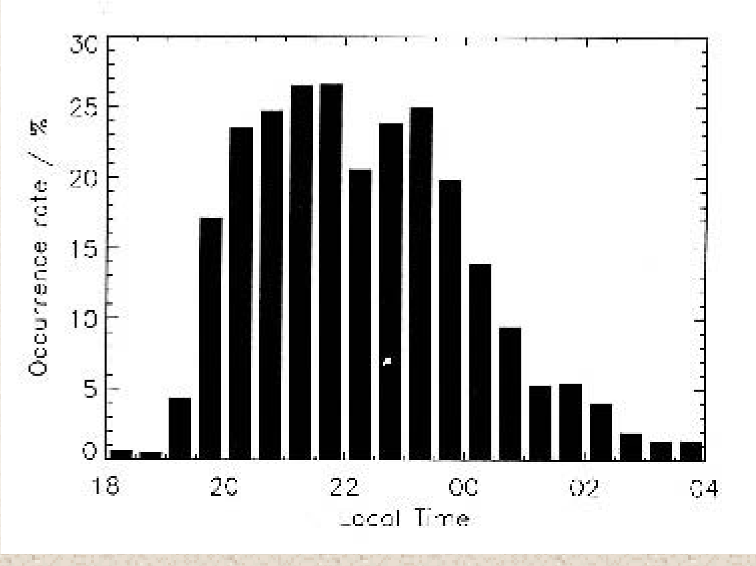

Stolle et al., 2006

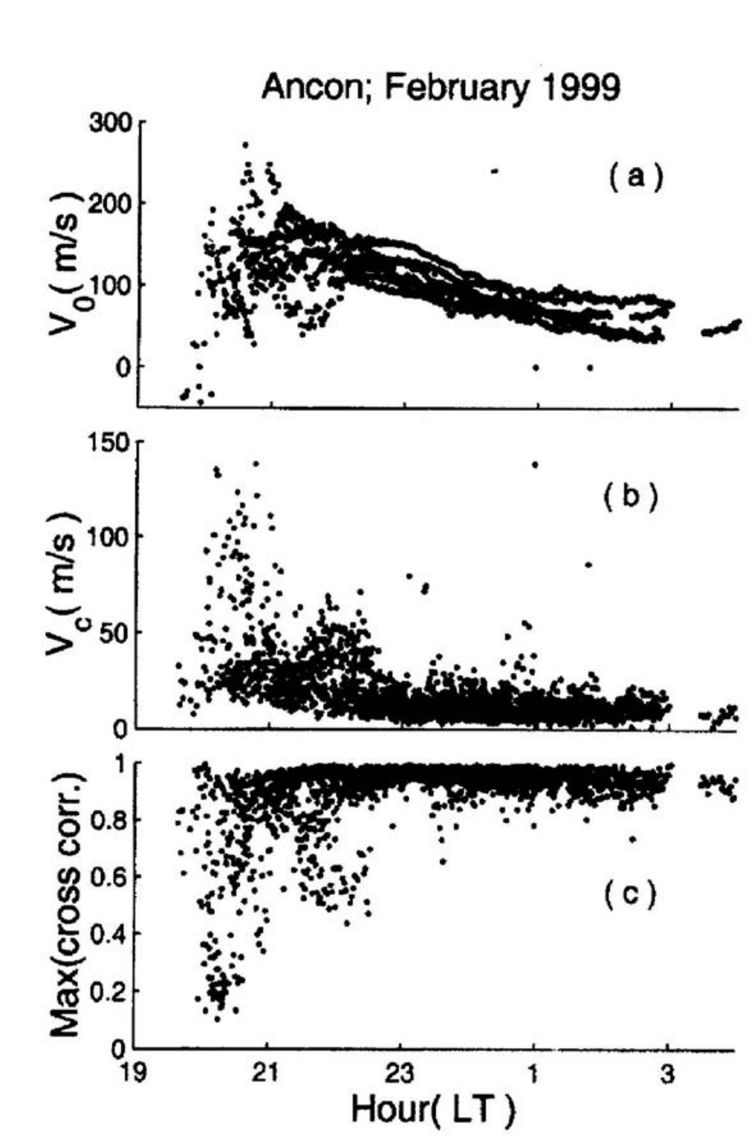

Electric and magnetic field perturbations associated with the instability follow the same LT pattern

Bhattacharyya et al., 2001

Bhattacharyya et al., 2006

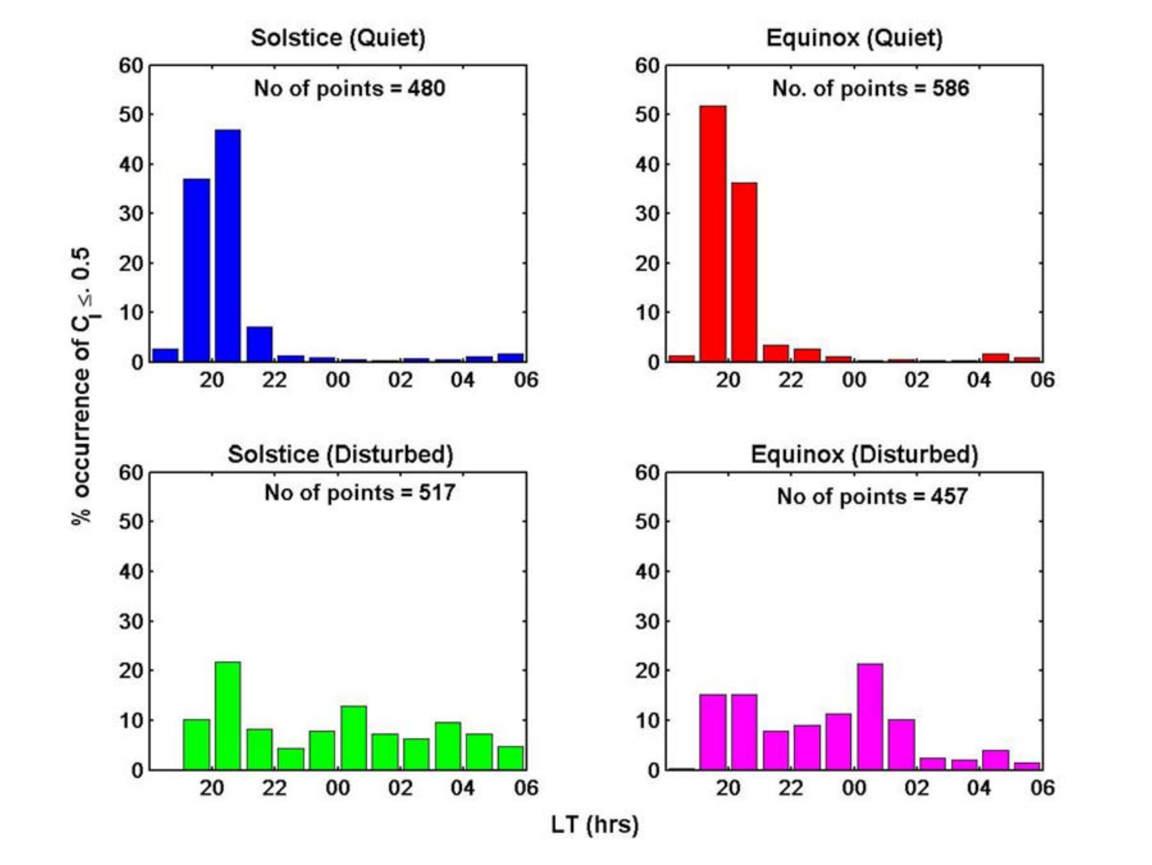

Spaced receiver signal decorrelation is used to identify equatorial plasma bubbles that are freshly generated due to magnetic activity, and hence their occurrence statistics.

Prompt penetration of magnetospheric electric field into equatorial ionosphere

Interplanetary Electric Field (IEF) values are calculated from the ACE observations of the solar wind velocity and IMF values and time-shifted to the magnetopause position.

$$\mathbf{IEF = - V_{sw} \; x \; B_{IMF}}$$

Daytime zonal electric fields at different longitudes are derived from the ΔH-inferred ExB drifts, where ΔH is derived from observations at equatorial and off-equatorial locations (Anderson et al., 2004)

Estimation of daytime low-latitude vertical ExB drift velocities from ground-based magnetometer observations

Peruvian Sector

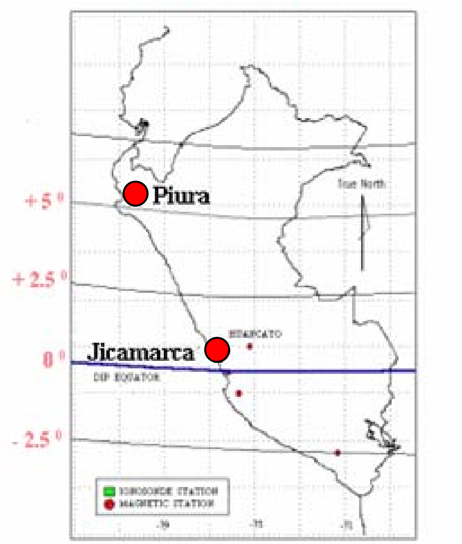

Philippine and Indonesian Sectors

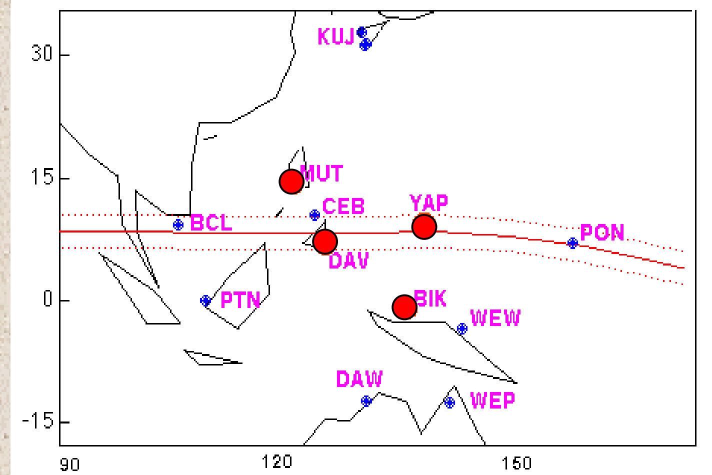

Indian Sector

Jicamarca
(Geog. 11.92° S; 283.13° E
Geomag. 0.8° N)

Piura
(Geog. 5.18° S; 279.36° E
Geomag. 6.8° N)

Davao
(Geog. 7° N; 125.4° E
Geomag. 1.32° S)

Muntinlupa
(Geog. 14.37° N; 121.02° E
Geomag. 6.39° N)

Yap
(Geog. 9.3° N; 138.5° E
Geomag. 0.5° N)

Biak
(Geog. 1.08° S; 136.0° E
Geomag. 9.74° S)

TIRUNELVELI
(Geog. 8.70° N; 76.95° E
Geomag. 0.46° S)

ALIBAG
(Geog. 18.62° N; 72.87° E
Geomag. 10° N)

Anderson et al., 2006

April 17 and 18, 2001

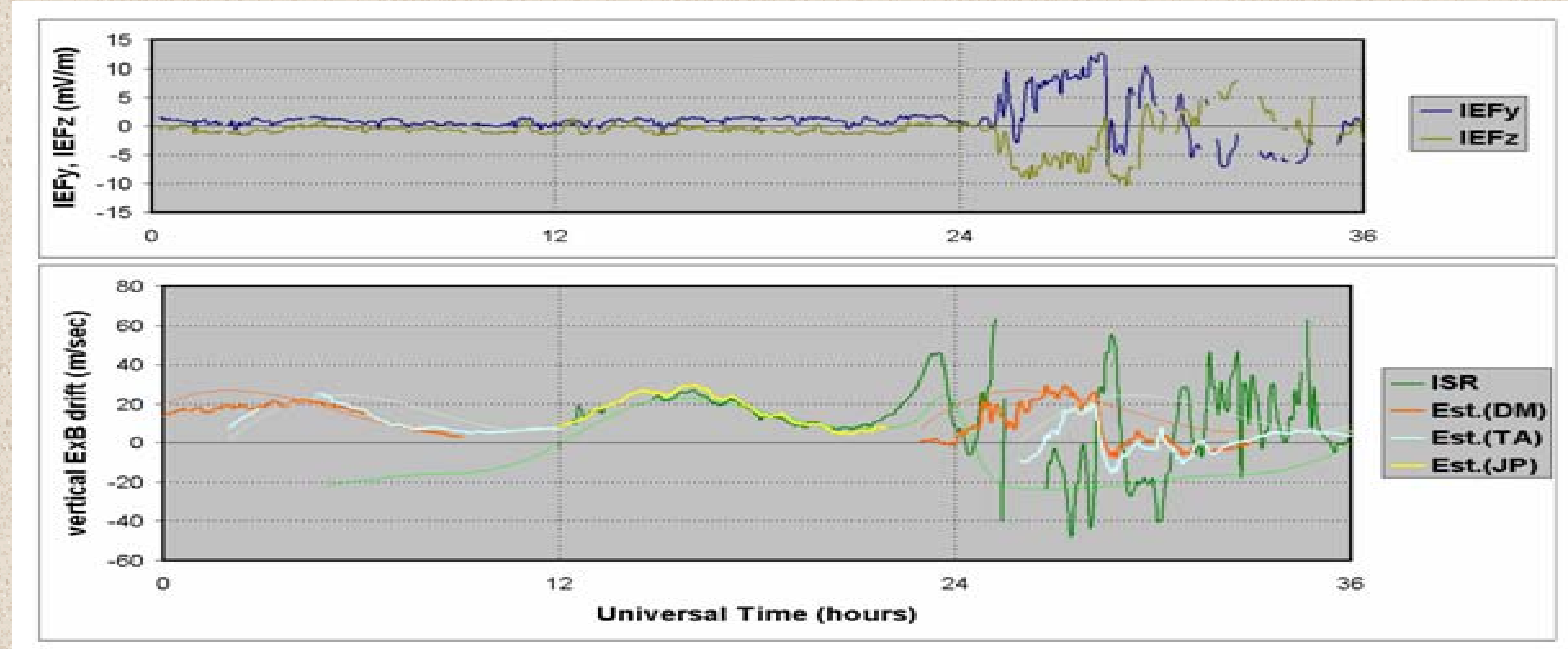

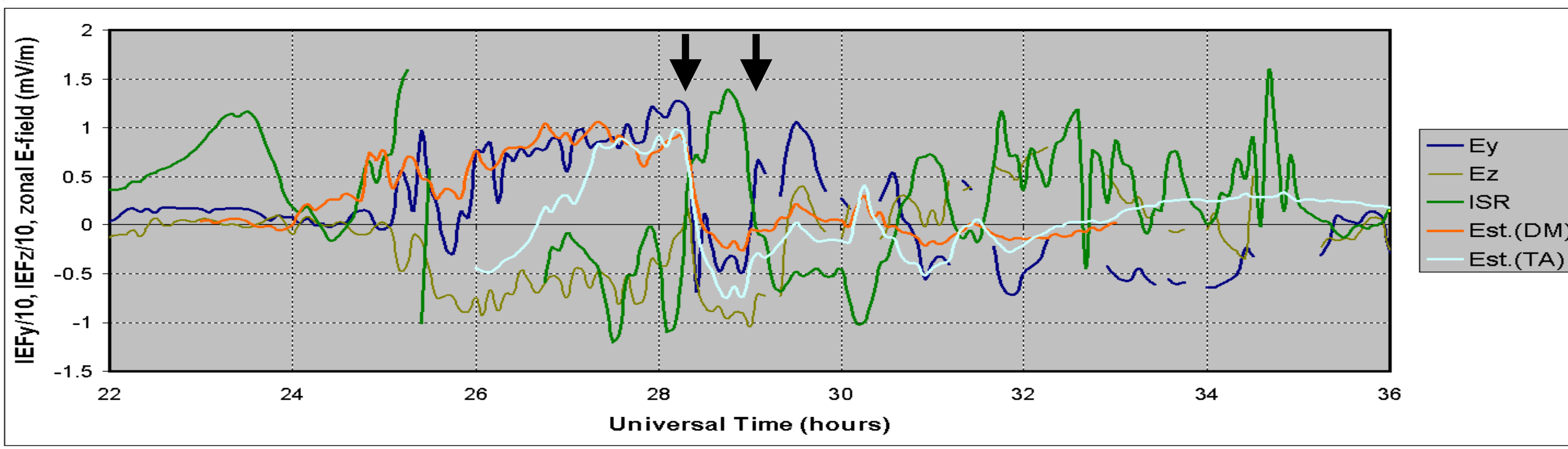

Anderson et al., 2006

April 17 and 18, 2002

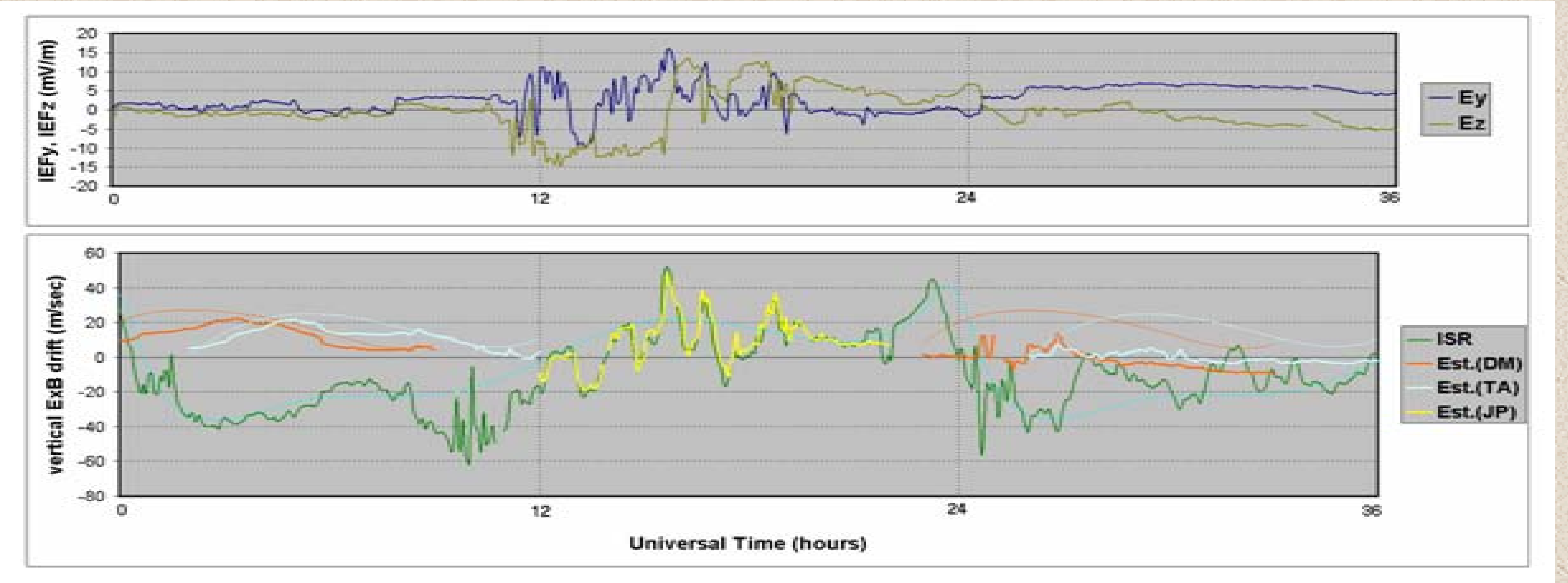

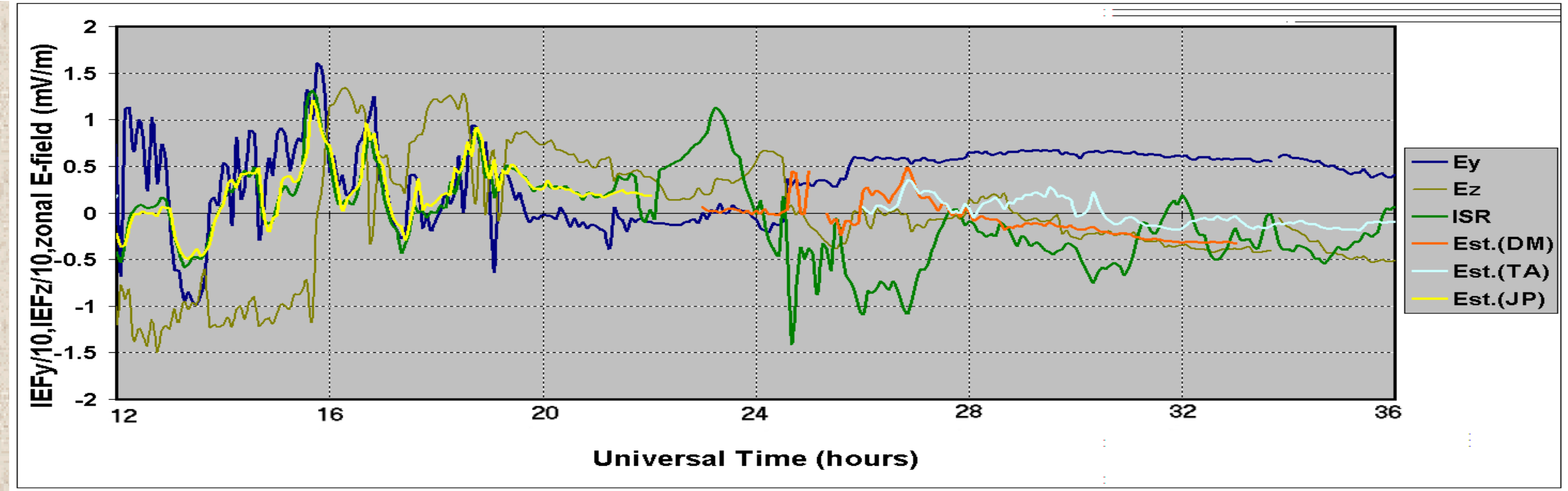

Anderson et al., 2006

CHAMP observation of EPBs on April 17, 2002 around 1920 UT

High-pass filtered vector magnetic field data from CHAMP in mean-field-aligned coordinates (z-axis aligned with mean magnetic field) and corresponding electron density data measured by PLP. Dashed line indicates the location of the dip equator.

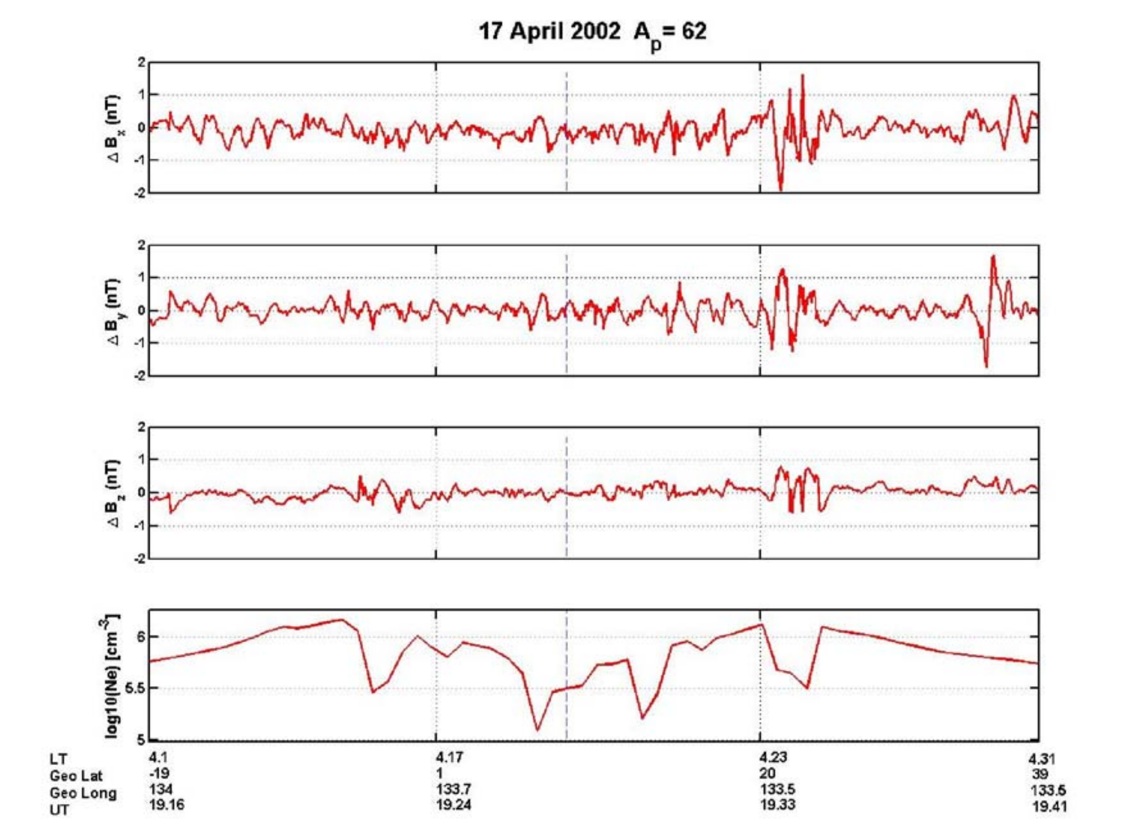

CHAMP observation of EPBs on January 11, 2002

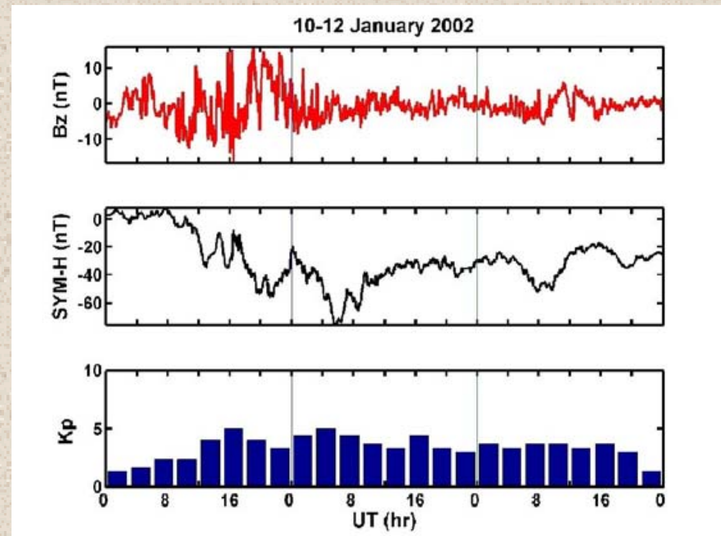

IMF B_Z and magnetic indices for 10-12 January, 2002

Fluctuations of ~ 4 nT in the magnetic field components transverse to the mean magnetic field aligned with the z-axis, are associated with EPBs generated on January 11, 2002.

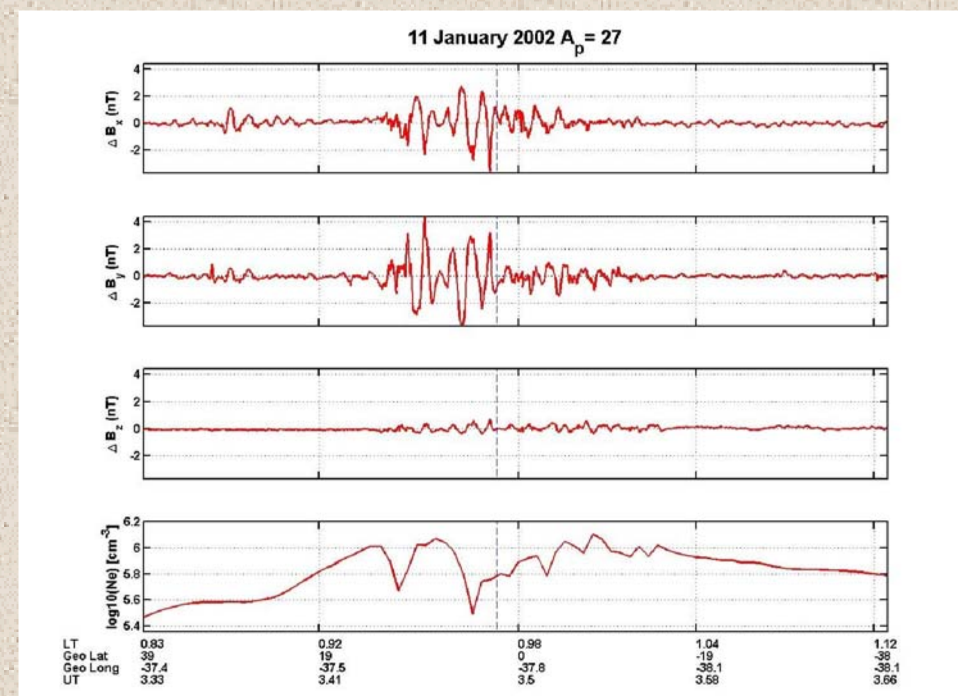

Use of *SWARM* data for EPB-related studies

- **Longitudinal variation in EPB characteristics.**

  Evolution of spatial structure in EPBs during quiet periods.
  Longitudinal variation in equatorial electric field disturbances caused by magnetic activity.

- **Vertical extent of EPBs under different conditions.**

  Change in characteristics of magnetic field fluctuations with height.

- Possible connection between meridional current system of the equatorial electrojet during dusk and the evening prereversal enhancement of equatorial F region vertical drift, which is a key parameter in the generation and evolution of EPBs.